中国光学（中英文） Chinese Optics 核心期刊

可实现宽带吸波稳定性提升的新型电阻等离子吸波结构

沈杨 芦志峰 郭亚坤 龙云飞 何睿 张哲瑞

Resistive plasmonic absorbing structures for stability enhancement of broadband absorption

SHEN Yang, LU Zhi-feng, GUO Ya-kun, LONG Yun-fei, HE Rui, Zhang Zhe-rui

引用本文:
沈杨, 芦志峰, 郭亚坤, 龙云飞, 何睿, 张哲瑞. 可实现宽带吸波稳定性提升的新型电阻等离子吸波结构[J]. 中国光学, 2024, 17(3): 683-692. doi: 10.37188/CO.EN-2023-0022
SHEN Yang, LU Zhi-feng, GUO Ya-kun, LONG Yun-fei, HE Rui, Zhang Zhe-rui. Resistive plasmonic absorbing structures for stability enhancement of broadband absorption[J]. *Chinese Optics*, 2024, 17(3): 683-692. doi: 10.37188/CO.EN-2023-0022

在线阅读 View online: https://doi.org/10.37188/CO.EN-2023-0022

您可能感兴趣的其他文章

Articles you may be interested in

双波长窄带宽介质超材料吸收器

Dual-wavelength narrow-bandwidth dielectric metamaterial absorber

中国光学（中英文）. 2021, 14(6): 1327 https://doi.org/10.37188/CO.2021-0075

基于非对称混合等离子体结构的双槽超紧凑偏振分束器

Double-slot ultra-compact polarization beam splitter based on asymmetric hybrid plasmonic structure

中国光学（中英文）. 2023, 16(5): 1215 https://doi.org/10.37188/CO.EN.2022-0028

亚波长尺度下混合等离子泄漏模式激光

Hybrid plasmonic leaky-mode lasing on subwavelength scale

中国光学（中英文）. 2021, 14(2): 397 https://doi.org/10.37188/CO.2020-0108

基于二氧化钒宽、窄带可切换的双功能超材料吸收器研究

Wide and narrow band switchable bi-functional metamaterial absorber based on vanadium dioxide

中国光学（中英文）. 2022, 15(2): 387 https://doi.org/10.37188/CO.2021-0174

石墨烯等离激元时间晶体中的慢光

Slow light in graphene plasmonic time crystals

中国光学（中英文）. 2022, 15(4): 845 https://doi.org/10.37188/CO.2021-0201

太赫兹人工表面等离子体共面激发与高*Q*传感

Coplanar excitation of terahertz spoof surface plasmon and high-*Q* sensing

中国光学（中英文）. 2023, 16(4): 933 https://doi.org/10.37188/CO.2022-0204

文章编号 2097-1842(2024)03-0683-10

Resistive plasmonic absorbing structures for stability enhancement of broadband absorption

SHEN Yang[1*], LU Zhi-feng[1], GUO Ya-kun[1], LONG Yun-fei[1], HE Rui[2], Zhang Zhe-rui[3]
(1. *Satellite Maritime Tracking and Controlling Department*, *Jiangyin* 214400, *China*;
2. *Aerospace System Department of Strategic Support Force of the People's Liberation Army of China*, *Beijing* 100193, *China*;
3. *Nanjing Research Institute of Electronic Technology*, *Nanjing* 210008, *China*)
* *Corresponding author*, *E-mail*: *shenyang*508@126.*com*

Abstract: Broadband absorption performance in resistive metamaterial absorbers (MA) has always been disturbed by its ohmic sheet element. We propose a comprehensive scheme based on integrating resistive MA and plasmonic structure (PS) to enhance the stable absorption performance. Theoretical investigation indicated that the PS can inspire multi-resonance based on dispersion engineering, and that the localized electric field takes effect on the surface of the ohmic sheet accordingly. Simulation and experimental measurement demonstrated that the proposed resistive plasmonic absorbing structures (PAS) can achieve stable and highly efficient absorption within the frequency band from 7.8 to 40.0 GHz with the ohmic sheet ranging from 100 to 250 Ω/sq. In conclusion, the proposed integration of PS and resistive MA provides an efficient pathway to optimize performance for various applications.

Key words: metamaterial absorber; plasmonic structure; broadband absorption; dispersion engineering

可实现宽带吸波稳定性提升的新型电阻等离子吸波结构

沈 杨[1*], 芦志峰[1], 郭亚坤[1], 龙云飞[1], 何 睿[2], 张哲瑞[3]
(1. 中国卫星海上测控部, 江苏 江阴 214400;
2. 中国人民解放军战略支援部队航天系统部, 北京 100193;
3. 南京电子技术研究所, 江苏 南京 210008)

摘要: 电阻型吸波结构具有优异的宽带电磁吸波性能, 但电阻片方阻值对吸波结构宽带电磁吸波性能影响较大, 且在样品制备过程中较难精确控制。本文通过在电阻型吸波结构表面加载周期性人工等离子结构, 利用宽频带内激发的多重

收稿日期: 2023-09-02; **修订日期:** 2023-10-07
基金项目: 国家自然科学基金资助项目(No. 61471388, No. 61801509); 国家重点研发项目(No. 2017YFA0700201)
Supported by National Natural Science Foundation of China (No. 61471388, No. 61801509); National Key R & D Program of China (No. 2017YFA0700201)

等离子谐振，实现高效宽带色散调控，进而获得电阻型吸波材料表面局域场增强效应，提升宽带电磁吸波的稳定性。仿真与试验结果表明，当电阻片方阻值在 100~250 Ω/sq 内变化时，该电阻型等离子吸波结构在 7.8~40.0 GHz 频段内的吸收效率高于 90% 以上，具有连续宽带电磁吸波能力。该设计方案提供了一种加载人工等离子结构用于强化吸波超材料综合性能的设计思路，对复合型吸波超材料设计具有一定的启发。

关　键　词：超材料吸波体；等离子结构；宽带吸波；色散调控

中图分类号：TB34　　**文献标志码：**A　　**doi：**10.37188/CO.EN-2023-0022

1 Introduction

Pursuing highly efficient broadband absorption performance has always been a central focus in the electromagnetic absorbing materials and devices community. Remarkably, metamaterials have provided unprecedented material options to achieve near-perfect absorption performance due to their optimization of impedance-matching characteristics, enabling extensive applications in the fields of stealth technique[1-2], energy harvesting[3-5], thermal emission control[6-8], image sensing[9-11], and so on. Early research indicated that an MA-based metal-insulator-metal configuration can flexibly control its electric or magnetic resonance to achieve near-perfect absorption[12]. Then, with the development of subwavelength structure, a series of MAs with single-, dual-, and multi-band absorption were raised gradually, contributing to the continued boom in MA research[13-21].

Achieving broadband absorption has long been an important goal in MA application. Remarkably, the scheme of overlapping multiple absorption peaks into continuous ones in a spectrum was first proposed to achieve broadband MA. The multiple resonators based on metal-insulator-metal configuration were assembled in the same plane[22-25] or along the vertical direction[26-29]; however, when they were adopted, they faced challenges in meeting both broadband absorption requirements and maintaining a lightweight design simultaneously. Meanwhile, it has been shown that dispersion engineering of multiple resonances by loading special material can also provide an efficient approach to broadband MA[30-35]. For example, using the standing-up ohmic sheet as a subwavelength unit cell, no-planar resistive MA can excite absorption peaks with a smoother profile at adjacent frequencies in the extremely wide frequency band[30-32]. Owing to its strong ohmic loss, resistive MA based on an ohmic sheet exhibits extreme broadband absorption while remaining lightweight. However, the broadband absorption of resistive MA is easily disturbed by the resistance value of the ohmic sheet. Meanwhile, through further research on dispersion engineering, a metallic PS based on gradually varied wire arrays adhered to the side of a loss dielectric substrate has been demonstrated to inspire spoof surface plasmon polaritons (SSPPs) in microwave frequency, contributing more diversified broadband and highly efficient absorption performance[36-39]. By contrast, the proposed PAS offers clear advantages in optimizing broadband absorption performance comprehensively.

In this paper, we attempt to add the PS on the side of no-planar resistive MA to further improve the operating bandwidth, absorption efficiency, and performance stability. Our investigation shows that the multiple resonances with the enhanced electric field can be excited on the surface of the ohmic sheet. Therefore, more ohmic loss takes effect in resistive PAS by the efforts from the enhanced electric field and ohmic sheet, contributing to stability enhancement in broadband absorption. At last, two samples were fabricated according to the simulated models, and the agreement between simulation and measurement validated our comprehensive scheme. With the aid of two absorbing mechanisms, our strategy provides an efficient way to enhance the

compositive absorption performance, enabling a wide range of applications in radar stealth technology, electromagnetic shielding, energy harvesting, and so on.

2 Design of no-planar resistive MA

As mentioned above, resistive MA based on an ohmic sheet exhibits extreme broadband absorption and is lightweight. Here, we will first discuss no-planar resistive MA. As the schematic shows in Fig. 1(color online), the dielectric substrate with the thickness t_f and height d was employed to achieve a squared grid. The side length of each grid unit cell is p. Then, four trapezoid ohmic sheets were printed on the inside of the grid along the clockwise direction, and one side of each trapezoid ohmic sheet was always close to the side of the dielectric substrate. Each trapezoid ohmic sheet had the upper edge length a_1, the bottom edge length a_2, the height d, and the resistance value f_z. The square metal plate was employed as a backplane on the bottom. The metal used was copper with an electric conductivity of 5.8×10^7 S/m, and the permittivity of the dielectric substrate was $4.3(1-j\cdot0.025)$. When giving the aforementioned parameters as follows: p=6.0 mm, d=5.0 mm, t_f=0.8 mm, a_1=2.6 mm, a_2=17.6 mm, and f_z=250 Ω/sq. The simulated result shows that the proposed no-planar MA achieves broadband absorption at an efficiency of more than 90% in the frequency band from 10.6 to 40.0 GHz under the normal incidence. Notably, the broadband absorption performance of the proposed resistive MA is easily affected by the resistance value of the ohmic sheet. As shown in Fig. 1(c), with the increased f_z from 100 to 250 Ω/sq, the absorption bandwidth concentrating on lower frequency was accordingly decreased. Meanwhile, significant improvement of absorption efficiency was observed during the middle-frequency band around 16.1−23.4 GHz. Moreover, accurately controlling the resistance value of the ohmic sheet in scale manufacturing is difficult, making it hard to achieve stable and efficient broadband absorption by relying solely on the resistive MA method.

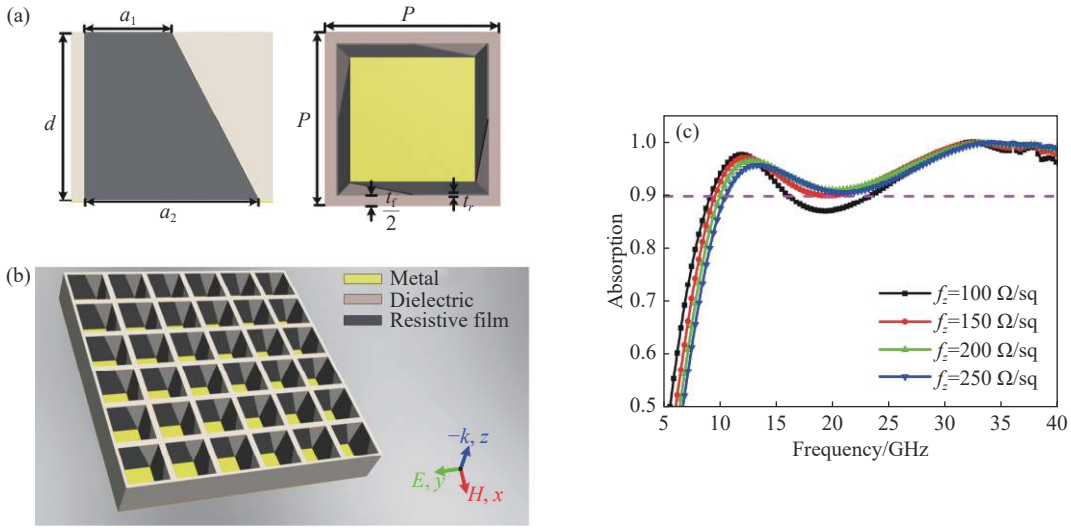

Fig. 1 (a) Schematic of no-planar resistive MA unit cell; (b) prospective view of no-planar resistive MA; (c) simulated absorption spectra of no-planar resistive MA under the normal incidence

3 Design of bent-wire-shaped PS

Meanwhile, Fig. 2(a) (color online) shows the schematic of the bent-wire-shaped structure made of metal wire and a dielectric substrate. The unit cell of the bent-wire-shaped structure was obtained by bending the straight wire 90° at the center point;

thus, the two components had the same length along horizontal and vertical directions. The bent wire with the total length l, width w, and thickness t_c was adhered to the dielectric substrate with the length a and height d. Then, the structural parameters were given as follows: a=6.0 mm, d=5.0 mm, t_f=0.4 mm, t_c=17.0 μm, w=0.1 mm. The dispersion relationship of the bent-wire-shaped structure with a different length l can be simulated by the eigenmode solver in CST Microwave Studio. In the modeling process, the metal was a perfect electric conductor, and the substrate had a relative dielectric constant of 4.3. To achieve an equivalent electromagnetic medium consisting of the bent-wire-shaped unit cell, the periodic boundary conditions were used along x and y while the plane wave with k-vector was incident along z direction. As the simulated results shown in Fig. 2(b) (color online), the ordinate represents the frequency change, while the horizontal coordinate represents the normalized k-vector change. Under the excitation of x-polarized waves, there are always two cut-off frequencies during the frequency of 0−30.0 GHz. All of the dispersion curves drift away from the light line and then approach their cut-off frequency as the k-vectors increase. Moreover, as shown in Tab. 1, with the increase in metal wire length from 7.0 mm to 10.0 mm, the first cut-off frequencies gradually decrease from 14.5 to 10.6 GHz, while the second cut-off frequencies gradually decrease from 24.9 to 20.4 GHz. This conclusively demonstrates that by adjusting the length of the metal wire, the cut-off frequency can be flexibly controlled in the bent-wire-shaped structure.

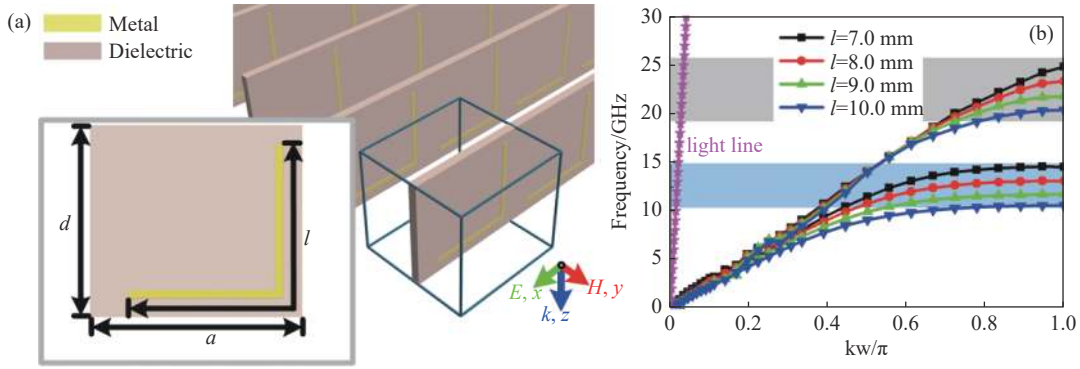

Fig. 2 (a) Schematic diagram and (b) dispersion relationship of the bent-wire-shaped structure

Tab. 1 Cut-off frequencies of the bent-wire-shaped structure with different lengths l

	l=7.0 mm	l=8.0 mm	l=9.0 mm	l=10.0 mm
The first cut-off frequency/GHz	14.5	13.1	11.8	10.6
The second cut-off frequency/GHz	24.9	23.4	21.8	20.4

On illumination, multiple bent wires with gradually varied lengths as well as fixed spacing were adhered to each side of the dielectric grid. Fig. 3(a) (color online) shows the longest bent wire had the length l_2=9.9 mm, comprised of a vertical section of 4.9 mm and a horizontal section of 5.0 mm. The following twenty-four bent wires with the same reduced length of 0.4 mm were also adhered to the dielectric substrate. For each bent wire array, the width, the period, and the thickness of the meandered wire were w=0.1 mm, s=0.2 mm, and t_c=17.0 μm, respectively. The period of the adjacent bent wire was always s=0.2 mm. Then, the achieved metal-dielectric combinations were rolled up as squared unit cells. The side length of the squared one was p=9.2 mm. The dielectric substrate was t_f=0.8 mm thick and d=10.0 mm tall. The backplane of bent-wire-shaped PS was air and the S-parameter spectra were calculated by the commercial software of CST Microwave Studio. As shown in Fig. 3(b) (color online), there was broadband suppression of more than 5 dB in the reflection spectrum from

9.5 GHz to 40.0 GHz and transmission spectrum from 17.0 GHz to 40.0 GHz under the normal incidence. Accordingly, the absorption spectrum of bent-wire-shaped PS can be obtained based on $A(\omega) = 1-R(\omega)-T(\omega) = 1-|S_{21}|^2-|S_{11}|^2$, where $A(\omega)$, $|S_{11}|^2$, and $|S_{21}|^2$ are the absorbance, reflectivity, and transmissivity, respectively. As shown in Fig. 3(c), the results demonstrate that bent-wire-shaped PS can achieve almost continuous absorption with an efficiency of more than 80% in the frequency band from 10.3 to 40.0 GHz.

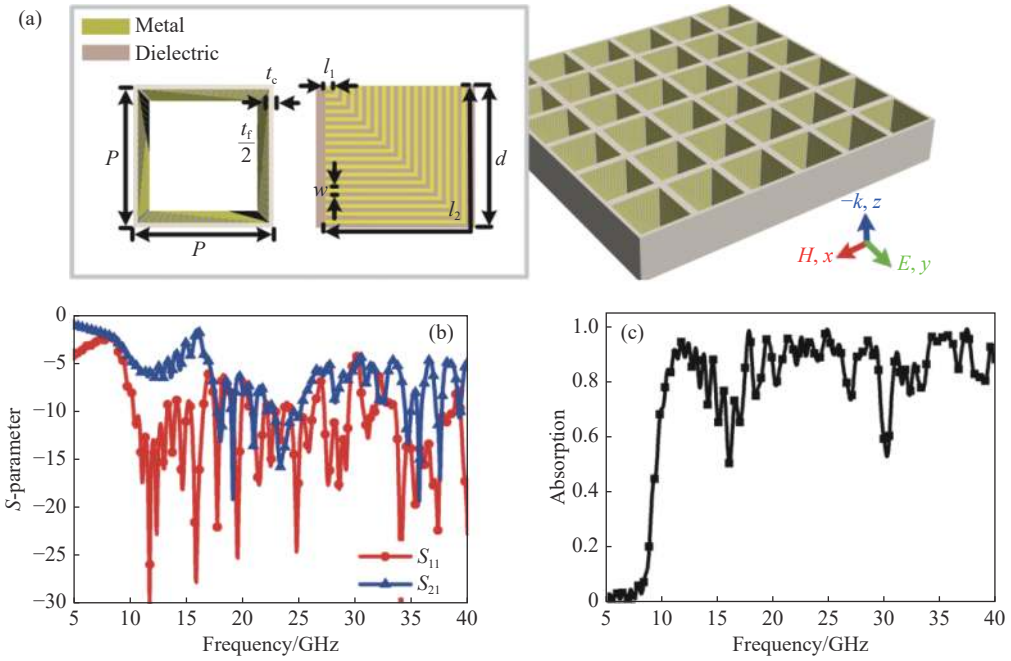

Fig. 3 (a) Schematic diagram of bent-wire-shaped PS; (b) reflection and transmission spectra of bent-wire-shaped PS under the normal incidence; (c) absorption spectra of bent-wire-shaped PS

4 Designs and discussions

Owing to the enhancement of the electric field inspired by dispersion engineering, bent-wire-shaped PS was loaded into no-planar resistive MA to further improve the operating bandwidth, absorption efficiency, and stable absorption profile. As shown in Fig. 4 (color online), the trapezoid ohmic sheet was printed on each side of the dielectric grid, then the bent wire array was also printed on each ohmic sheet. For each unit cell, there were four ohmic sheets and four bent wire arrays which were always arranged clockwise. The side length of each unit cell was P. The thickness and the height of the dielectric substrate were t_f and d. For the trapezoid ohmic sheet, the upper edge length, the bottom edge length, the height, the thickness, and the resistance value are a_1, a_2, d, and f_z, respectively. For the bent wire array, the width, the period, and the thickness of the meandered wire are w, s, and t_c. Each array has twenty-five bent wires with lengths ranging from l_1 to l_2. When giving the aforementioned parameters as follows: p=6.0 mm, t_f=0.8 mm, d=5.0 mm, a_1=2.6 mm, a_2=17.6 mm, f_z=250 Ω/sq, w=0.1 mm, s=0.2 mm, t_c=17.0 μm l_1=0.2 mm and l_2=9.9 mm, the simulated result shows that the proposed resistive PAS can achieve broadband absorption with an efficiency of more than 90% during the frequency band from 7.8 GHz to 40.0 GHz, which is a significant improvement of lower-frequency absorption as compared with resistive MA. Here, the comprehensive evaluations of their broadband absorption can be carried out by the figure of merit (FOM). According to the Rozanov limit[40-41], the FOM is calculated following the relation FOM=$d/(\lambda_L-\lambda_H)$, where d is

the sample thickness, λ_L and λ_H are the lower-bound wavelength and high-bound wavelength of the absorption band. Hereby, the smallest value of FOM is always expected for desired broadband absorption. Calculated results show that the FOM values of resistive MA and resistive PAS are 0.24 and 0.16. The resistive PAS proposed in this paper exhibits outstanding improvement in broadband absorption, especially for low-frequency absorption. Furthermore, the simulated absorption spectra in Fig. 5(a) (color online) show that the absorption bandwidth remains almost constant as the resistance value f_z decreases from 250 Ω/sq to 100 Ω/sq.

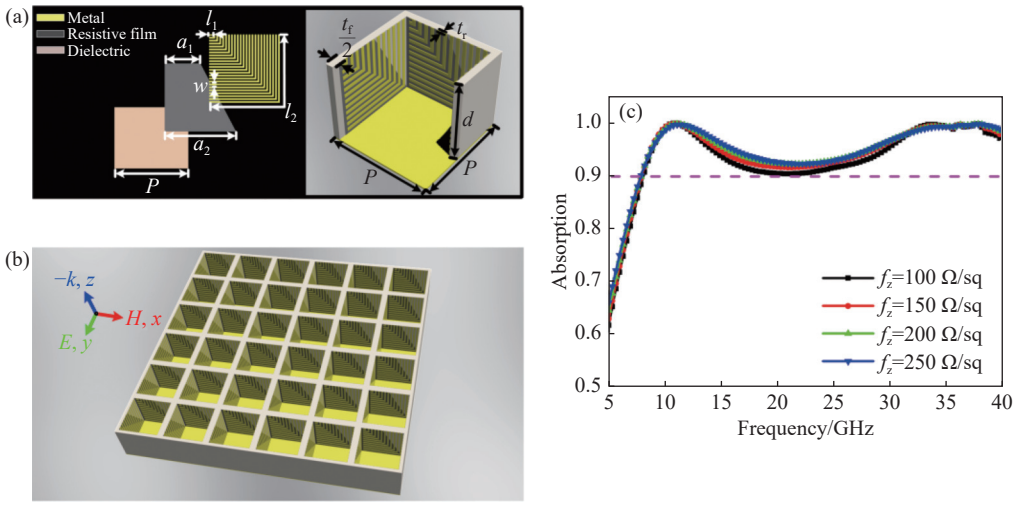

Fig. 4 (a) Schematic diagram of resistive PAS unit cell; (b) prospective view of resistive PAS; (c) simulated absorption spectra of the proposed resistive PAS under the normal incidence

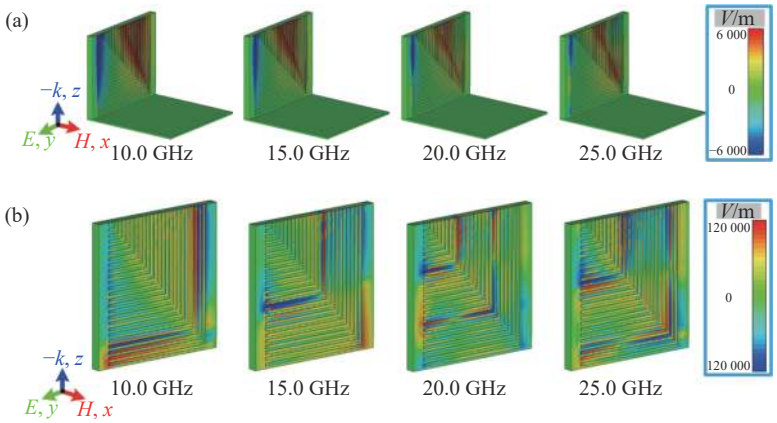

Fig. 5 Electric field E_y distributions of (a) resistive PAS and (b) bent-wire-shaped PS in the *y*-*z* plane at the frequencies of 10.0, 15.0, 20.0, and 25.0 GHz

To better understand its absorption principle, the electric field E_y distributions of bent-wire-shaped PS were monitored at the frequencies of 10.0, 15.0, 20.0, and 25.0 GHz in Fig. 5(b) (color online). For the lower frequency of 10.0 GHz, one resonance corresponding to several adjacent bent wires was obtained, which contributed to the clear enhancement of the local electric field. The enhanced electric field on the metal-dielectric interface took effect with the loss from the dielectric substrate, and highly effective absorption was achieved following the relation $P_{abs}=1/2(\omega\varepsilon''+\sigma)|E|^2$, where ω was the angular frequency, ε'' was the imaginary part of permittivity, r was the conductivity, and E was the total electric field. For the higher frequencies of 15.0 GHz, 20.0 GHz, and 25.0 GHz,

there were always two kinds of resonances corresponding to the entire wire on the top layer and the remaining half wire on the bottom layer. The two resonances worked together to contribute highly efficient absorption at each frequency. Each resonant frequency was always consistent with the former cut-off frequency. Also, the electric field E_y distributions of resistive PAS were also monitored at the frequencies of 10.0, 15.0, 20.0, and 25.0 GHz, as shown in Fig. 5(a). Owing to the dispersion engineering of bent-wire-shaped PS, the inspired localized surface-wave-like electromagnetic oscillation took effect at those frequency points on the loss substrate of the ohmic sheet, and thus broadband and highly efficient absorption performance was achieved. Therefore, it can be concluded that the resistive PMA proposed in this paper achieves optimal performance with comprehensive consideration of the operating bandwidth, absorption efficiency, and stable absorption profile.

5 Experimental validation

To validate the proposed resistive PAS, two samples with the ohmic sheet of f_z=100 Ω/sq and f_z=250 Ω/sq were fabricated, and the other structure parameters remained exactly the same. As shown in Fig. 6, one sample with the ohmic sheet f_z=100 Ω/sq had the dimension of 140.0 mm×140.0 mm, including of 196 unit cells. In the fabrication process, the rectangular dielectric strips were cut with periodical grooves by a numerical control tool and then assembled on the copper plane through a squared grid method. On each side of the dielectric substrate, the metallic bent wire arrays were printed at regular intervals by circuit board printing technology. Meanwhile, the ohmic sheets with the resistance values of f_z=100 Ω/sq and f_z=250 Ω/sq were printed on the ultra-thin dielectric films respectively by screen printing technology and then adhered to the metal-dielectric grid at regular intervals by epoxy resin. The experimental measurements of the two models were performed in an anechoic chamber. The measurement system was based on an Agilent 8720ET network analyzer with five pairs of broadband antenna horns working in the frequency bands of 5−8, 8−12, 12−18, 18−26, and 26−40 GHz. Figs. 7(a) and 7(b) (color online) present the measured absorption spectra along with their simulated results. The strong agreement between simulation and measurement further validates the design concept outlined in this paper.

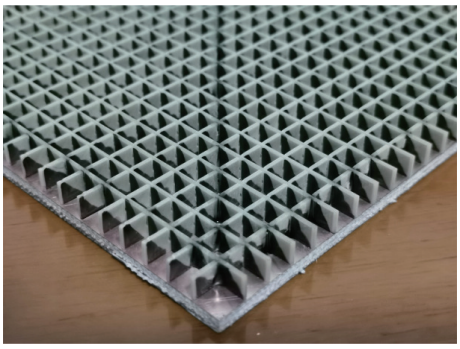

Fig. 6 Fabricated sample of resistive PAS with the ohmic sheet f_z=100 Ω/sq

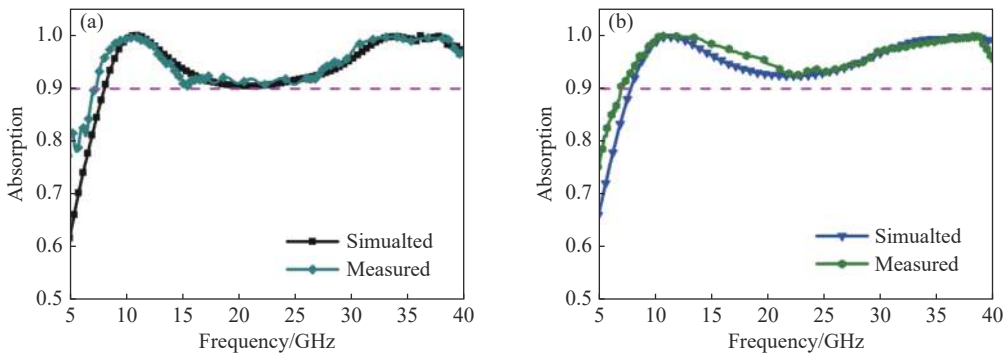

Fig. 7 Simulated and measured absorption spectra of resistive PAS with an ohmic sheet (a) f_z=100 Ω/sq and (b) f_z=250 Ω/sq

6 Conclusion

In summary, we describe the achievement of resistive PAS based on a comprehensive scheme that provided an efficient path to absorption performance optimization, contributing more potential applications. The proposed resistive PAS was obtained based on the integration of no-planar resistive MA and plasmonic structure. The theoretical investigation demonstrated that multi-resonance can be excited based on spatial dispersion engineering of PS, causing the localized electric field to take effect on the surface of the resistive ohmic sheet. The proposed approach counters the defect of the broadband absorption performance being easily affected by its constituent ohmic sheet in resistive MA. As proof, two samples were fabricated according to the simulated models. The strong agreement between simulations and experimental measurements demonstrates that resistive PAS can always achieve broadband and highly efficient absorption performance during the frequency band from 8.0 to 40.0 GHz with the ohmic sheet ranging from 100 to 250 Ω/sq.

References:

[1] WATTS C M, LIU X L, PADILLA W J. Metamaterial electromagnetic wave absorbers[J]. *Advanced Materials*, 2012, 24(23): OP98-OP120.

[2] GLYBOVSKI S B, TRETYAKOV S A, BELOV P A, *et al*.. Metasurfaces: from microwaves to visible[J]. *Physics Reports*, 2016, 634: 1-72.

[3] TONG J K, HSU W C, HUANG Y, *et al*.. Thin-film ‘thermal well’ emitters and absorbers for high-efficiency thermophotovoltaics[J]. *Scientific Reports*, 2015, 5: 10661.

[4] ATALLA M R M, ATTIA M T. On the broadband continuous polarization-independent excitation of surface-plasmon-polariton waves for energy-harvesting applications[J]. *Journal of the Optical Society of America B*, 2017, 34(2): 270-278.

[5] WANG ZH Y, TONG ZH, YE Q X, *et al*.. Dynamic tuning of optical absorbers for accelerated solar-thermal energy storage[J]. *Nature Communications*, 2017, 8(1): 1478.

[6] DIEM M, KOSCHNY T, SOUKOULIS C M. Wide-angle perfect absorber/thermal emitter in the terahertz regime[J]. *Physical Review B*, 2008, 79(3): 033101.

[7] MASON J A, SMITH S, WASSERMAN D. Strong absorption and selective thermal emission from a midinfrared metamaterial[J]. *Applied Physics Letters*, 2011, 98(24): 241105.

[8] SHEN Y, ZHANG J Q, PANG Y Q, *et al*.. Transparent broadband metamaterial absorber enhanced by water-substrate incorporation[J]. *Optics Express*, 2018, 26(12): 15665-15674.

[9] LANDY N I, BINGHAM C M, TYLER T, *et al*.. Design, theory, and measurement of a polarization-insensitive absorber for terahertz imaging[J]. *Physical Review B*, 2009, 79(12): 125104.

[10] BAKIR M, KARAASLAN M, UNAL E, *et al*.. Microwave metamaterial absorber for sensing applications[J]. *Opto-Electronics Review*, 2017, 25(4): 318-325.

[11] LIU N, MESCH M, WEISS T, *et al*.. Infrared perfect absorber and its application as plasmonic sensor[J]. *Nano Letters*, 2010, 10(7): 2342-2348.

[12] LANDY N I, SAJUYIGBE S, MOCK J J, *et al*.. Perfect metamaterial absorber[J]. *Physical Review Letters*, 2008, 100(20): 207402.

[13] TAO H, BINGHAM C M, PILON D, *et al*.. A dual band terahertz metamaterial absorber[J]. *Journal of Physics D:Applied Physics*, 2010, 43(22): 225102.

[14] CUI Y X, XU J, HUNG FUNG K, *et al*.. A thin film broadband absorber based on multi-sized nanoantennas[J]. *Applied Physics Letters*, 2011, 99(25): 253101.

[15] HUANG L, CHOWDHURY D R, RAMANI S, *et al*.. Experimental demonstration of terahertz metamaterial absorbers with a broad and flat high absorption band[J]. *Optics Letters*, 2012, 37(2): 154-156.

[16] TUNG B S, KHUYEN B X, VAN DUNG N, *et al*.. Multi-band near-perfect absorption via the resonance excitation of dark meta-molecules[J]. *Optics Communications*, 2015, 356: 362-367.

[17] CHENG Y ZH, CHENG ZH Z, MAO X S, *et al*.. Ultra-thin multi-band polarization-insensitive microwave metamaterial absorber based on multiple-order responses using a single resonator structure[J]. *Materials*, 2017, 10(11): 1241.

[18] ZHAO L, LIU H, HE ZH H, *et al*.. Design of multi-narrowband metamaterial perfect absorbers in near-infrared band based on resonators asymmetric method and modified resonators stacked method[J]. *Optics Communications*, 2018, 420: 95-103.

[19] LI SH Y, AI X CH, WU R H, *et al*.. Enhancement of multi-band absorption based on compound structure metamaterials [J]. *Optics & Laser Technology*, 2019, 115: 239-245.

[20] MAO Q J, FENG CH Z, YANG Y ZH. Design of tunable multi-band metamaterial perfect absorbers based on magnetic polaritons[J]. *Plasmonics*, 2019, 14(2): 389-396.

[21] HANNAN S, ISLAM M T, SAHAR N M, *et al*.. Modified-segmented split-ring based polarization and angle-insensitive multi-band metamaterial absorber for X, Ku and K band applications[J]. *IEEE Access*, 2020, 8: 144051-144063.

[22] GOMON D, SEDYKH E, RODRÍGUEZ S, *et al*.. Influence of the geometric parameters of the electrical ring resonator metasurface on the performance of metamaterial absorbers for terahertz applications[J]. *Chinese Optics*, 2018, 11(1): 47-59.

[23] SHEN Y, PEI ZH B, PANG Y Q, *et al*.. Phase random metasurfaces for broadband wide-angle radar cross section reduction[J]. *Microwave and Optical Technology Letters*, 2015, 57(12): 2813-2819.

[24] TRAN M C, PHAM V H, HO T H, *et al*.. Broadband microwave coding metamaterial absorbers[J]. *Scientific Reports*, 2020, 10(1): 1810.

[25] MUDACHATHI R, TANAKA T. 3D conical helix metamaterial–based isotropic broadband perfect light absorber[J]. *Optics Express*, 2019, 27(19): 26369-26376.

[26] CUI Y X, FUNG K H, XU J, *et al*.. Ultrabroadband light absorption by a sawtooth anisotropic metamaterial slab[J]. *Nano Letters*, 2012, 12(3): 1443-1447.

[27] DING F, CUI Y X, GE X CH, *et al*.. Ultra-broadband microwave metamaterial absorber[J]. *Applied Physics Letters*, 2012, 100(10): 103506.

[28] LIU SH, CHEN H B, CUI T J. A broadband terahertz absorber using multi-layer stacked bars[J]. *Applied Physics Letters*, 2015, 106(15): 151601.

[29] JI SH J, JIANG CH X, ZHAO J, *et al*.. An ultra-broadband metamaterial absorber with high absorption rate throughout the X-band[J]. *Physica Status Solidi (B)*, 2019, 256(11): 1900069.

[30] SHEN Y, PEI ZH B, PANG Y Q, *et al*.. An extremely wideband and lightweight metamaterial absorber[J]. *Journal of Applied Physics*, 2015, 117(22): 224503.

[31] TANG J Y, XIAO ZH Y, XU K K, *et al*.. Polarization-controlled metamaterial absorber with extremely bandwidth and wide incidence angle[J]. *Plasmonics*, 2016, 11(5): 1393-1399.

[32] HU D W, CAO J, LI W, *et al*.. Optically transparent broadband microwave absorption metamaterial by standing-up closed-ring resonators[J]. *Advanced Optical Materials*, 2017, 5(13): 1700109.

[33] YE D X, WANG ZH Y, XU K W, *et al*.. Ultrawideband dispersion control of a metamaterial surface for perfectly-matched-layer-like absorption[J]. *Physical Review Letters*, 2013, 111(18): 187402.

[34] ZHANG H F, JING Y, ZHANG H, *et al*.. Design of an ultra-broadband absorber based on plasma metamaterial and lumped resistors[J]. *Optical Materials Express*, 2018, 8(8): 2103-2113.

[35] MA X, TIAN F, LI X Y, *et al*.. Broadband with enhanced oblique incidence metamaterial absorber[J]. *Materials Research Express*, 2020, 7(9): 095803.

[36] PANG Y Q, WANG J F, MA H, *et al*.. Spatial *k*-dispersion engineering of spoof surface plasmon polaritons for customized absorption[J]. *Scientific Reports*, 2016, 6: 29429.

[37] SHEN Y, ZHANG J Q, MENG Y Y, *et al*.. Merging absorption bands of plasmonic structures via dispersion engineering[J]. *Applied Physics Letters*, 2018, 112(25): 254103.

[38] SHEN Y, ZHANG J Q, WANG J F, *et al*.. Multistage dispersion engineering in a three-dimensional plasmonic structure for outstanding broadband absorption[J]. *Optical Materials Express*, 2019, 9(3): 1539-1550.

[39] SHEN Y, ZHANG J Q, WANG W J, *et al*.. Overcoming the pixel-density limit in plasmonic absorbing structure for

broadband absorption enhancement[J]. *IEEE Antennas and Wireless Propagation Letters*, 2019, 18(4): 674-678.

[40] ROZANOV K N, STAROSTENKO S N. Numerical study of bandwidth of radar absorbers[J]. *The European Physical Journal Applied Physics*, 1999, 8(2): 147-151.

[41] ROZANOV K N. Ultimate thickness to bandwidth ratio of radar absorbers[J]. *IEEE Transactions on Antennas and Propagation*, 2000, 48(8): 1230-1234.

Author Biographics:

Shen Yang (1990—), Ph.D., Engineer, Satellite Maritime Tracking and Controlling Department. His research interests concentrate on the basic theory and application of metamaterials in the field of electromagnetic waves, materials engineering, and surface plasmons. E-mail: shenyang508@126.com